DFT Study of Hydrogen Adsorption on Palladium Decorated Graphene

ARTICLE *in* THE JOURNAL OF PHYSICAL CHEMISTRY C · FEBRUARY 2011

Impact Factor: 4.77 · DOI: 10.1021/jp110067w

5 AUTHORS, INCLUDING:

Estefanía Germán
Universidad Nacional del Sur
21 PUBLICATIONS **140** CITATIONS
SEE PROFILE

María A. Volpe
Planta Piloto de Ingeniería Química
40 PUBLICATIONS **750** CITATIONS
SEE PROFILE

Graciela Brizuela
Universidad Nacional del Sur
14 PUBLICATIONS **151** CITATIONS
SEE PROFILE

Available online at www.sciencedirect.com

SciVerse ScienceDirect

journal homepage: www.elsevier.com/locate/he

Hydrogen adsorption on palladium dimer decorated graphene: A bonding study

I. López-Corral [a], E. Germán [a], A. Juan [a,*], M.A. Volpe [b], G.P. Brizuela [a]

[a] Departamento de Física and Instituto de Física del Sur, Universidad Nacional del Sur-CONICET, Av. Alem 1253, 8000 Bahía Blanca, Argentina

[b] Departamento de Química and Planta Piloto de Ingeniería Química, Universidad Nacional del Sur-CONICET, camino de La Carrindanga Km. 7, 8000 Bahía Blanca, Argentina

ARTICLE INFO

Article history:
Received 18 October 2011
Received in revised form
8 January 2012
Accepted 10 January 2012
Available online 17 February 2012

Keywords:
Hydrogen
Graphene
Carbon nanotubes
Palladium
DFT
Bonding

ABSTRACT

We report a density-functional theory study of dihydrogen adsorption on a graphene sheet functionalized with palladium dimers considering different adsorption sites on the carbon surface and both molecular and dissociative Pd_2H_2 coordination structures. Our results show that a $(PdH)_2$ ring without an H–H bond and not dissociative $Pd_2(H_2)$ complexes are stable adsorbed systems with more elongated Pd–Pd and Pd–H bonds compared to the unsupported configurations caused by C–Pd interactions. In contrast, individual Pd atoms supported on graphene react with H_2 to form only a $Pd(H_2)$ complex with a relaxed but not dissociated H–H bond. We also performed the Mulliken analysis to study the bonding mechanism during the adsorption process. In most cases, we found donor-acceptor C–Pd and Pd–H interactions in which C 2*p*, Pd 5*s*, and H 1*s* orbitals played an important role. We also found that the adsorption of a second Pd atom close to a PdH_2 system destabilizes the H–H bond. In this work we contribute to shed more light on the relation between Pd clustering and the possibility of hydrogen storage in graphene-based materials.

1. Introduction

The development of a hydrogen-based economy requests effective hydrogen storage media. Hydrogen compression and liquefaction cannot meet the storage target proposed by the U.S. Department of Energy, so attention has mainly been focused on hydrogen adsorption in porous media. Hydrogen physical adsorption storage has reversibility and fast kinetics in comparison to chemical adsorption, which usually needs high release temperatures. Nowadays, researchers are exploring a multitude of carbon-based materials, such as activated carbons (ACs), carbon nanotubes (CNTs), carbon nanofibers (CNFs), and graphene layers because of their light weight and high stability. However, hydrogen molecules physisorb at the surface or inside the pores of the carbon material by weak dispersion (Van der Waals) forces, and, thus, efficient storage is only possible at cryogenic temperatures [1,2].

A way for increasing hydrogen storage capacity at ambient conditions is by adding transition metal (TM) atoms to carbon structures, thus obtaining composite materials that combine physical and chemical adsorption processes. This activation may be explained through the spillover mechanism [3] which involves the dissociative chemisorption of H_2 molecules on TM particles and the migration of the resulting H atoms to remote surface sites, otherwise inaccessible to molecular

* *Corresponding author*. Tel./fax: +54 291 4595142.
E-mail address: cajuan@criba.edu.ar (A. Juan).

0360-3199/$ – see front matter Copyright © 2012, Hydrogen Energy Publications, LLC. Published by Elsevier Ltd. All rights reserved.
doi:10.1016/j.ijhydene.2012.01.039

hydrogen. Several experimental studies have reported enhanced hydrogen uptakes by carbon structures doped with TMs, for example Pt [4–6], Ni [7–9] or Pd [10–21], that are better than the uptake of each single component. Yang et al. [15–17] also found that providing carbon bridges between the spillover source and the carbon receptor doubles or even triples hydrogen uptake. Besides chemisorption on exposed surface, Pd particles can also absorb hydrogen interstitially to form two hydride phases: α-PdH_x ($x \sim 0.02$) and β-PdH_x ($x \sim 0.67$) [22]. By using high pressure x-ray diffraction analysis *in situ*, Bhat et al. [23] suggest that a higher degree of Pd-carbon contacts for Pd particles embedded in a microporous carbon matrix destabilizes the H rich β-PdH_x phase and induces efficient transfer of H atoms from this phase to adsorption sites on carbon, contributing to enhanced hydrogen spillover.

Theoretical studies have predicted that carbon-supported single TM atoms could directly interact with several H_2 molecules to form the so-called Kubas complexes [24] with a binding energy in the region of 2–12 kcal mol^{-1}, that is acceptable for room temperature storage [25]. First-principle density-functional theory (DFT) calculations [8,26–29] showed that carbon-based materials decorated with light TMs, like Ti, Ni, Sc, and V should be capable of binding up to five hydrogen molecules per metal atom, developing a binding energy between 7 and 12 kcal mol^{-1} and a gravimetric density higher than 7 wt%. In contrast, isolated heavy TM atoms, such as Pt and Pd, could not induce the bonding of more than two H_2 molecules [30], thus resulting in lower hydrogen storage capacities. However, a recent DFT report [31] has shown that two adjacent Pd atoms adsorbed on a (8.0) single-walled (SW) CNT could bind up to five H_2 molecules, reaching a hydrogen density of ~3 wt%. Unfortunately, metallic clustering and phase segregation make TM nanoparticle uniform dispersion on carbon samples under practical conditions very difficult [32,33], therefore, the hydrogen uptake of carbon materials based on Kubas interaction cannot be experimentally proven.

Theoretical calculations have also shown that the size of metal particles configures, to a great extent, the thermodynamic properties of activated carbon structures toward hydrogen adsorption. For example, Sun et al. [34] have proposed that the clustering of Ti atoms adsorbed on a C_{60} fullerene not only changes the nature of hydrogen bonding, but also reduces its adsorption capacity because it inhibits the interaction of hydrogen with core metal atoms. On the other hand, Wagemans et al. [35] have found that the thermodynamic properties of Mg hydride can be destabilized if the size of the metallic particles is below 1 nm. Although it has been experimentally proven [20,36] that the decrease in size of carbon-supported Pd nanoparticles can change their hydrogen storage capacities, theoretical reports on the interaction between dihydrogen and Pd clusters adsorbed on carbon-based materials are still scarce.

In a previous work [37], we have analyzed the electronic structure and the bonding evolution involved in the adsorption of dihydrogen on a graphene sheet doped with single Pd atoms through DFT calculations, considering different molecular and dissociative PdH_2 complexes. We have verified that the most stable graphene-supported PdH_2 coordination structure is similar to the isolated Kubas complex, with a relaxed but not dissociated H–H bond. However, during the adsorption process, new C–Pd bonds are formed and the H–H bond becomes strengthened with respect to the free PdH_2 complex. Moreover, we found that the Pd–H bonds developed when atomic hydrogen is adsorbed are stronger than when originated in the dihydrogen bonding so that the spillover mechanism could also be related to the hydrogen uptake of Pd-doped graphene-based materials. In the present paper, we continue our earlier investigation by analyzing the interaction of a hydrogen molecule with a Pd_2 dimer adsorbed onto a graphene surface, as a model to study the Pd clustering effect on hydrogen storage. In particular, we focus on bonding interactions during molecular and dissociative adsorption of H_2 molecules on the carbon-supported Pd_2 dimer, including orbital occupation analysis.

2. Computational details

Electronic structure calculations were performed within the framework of the first-principle DFT [38,39] under the Perdew-Burke-Ernzerhof (PBE) form of the generalized gradient approximation (GGA) [40], including spin polarization. Simulations were performed using the SIESTA computer code [41,42], which adopts a linear combination of numerical localized atomic-orbital basis sets for the description of valence electrons. We chose a split-valence double-zeta basis set with a polarization function (DZP) for all the atoms [42,43]. Standard norm-conserving Troullier-Martins pseudopotentials [44] were used to describe the interaction between valence electrons and atomic core. The energy cut-off value for the real space integration mesh was 150 Ry for all the systems [41]. Sampling of the Brillouin Zone (BZ) for both bare graphene and Pd-functionalizated graphene was carried out with a Monkhorst-Pack regular grid of $20 \times 20 \times 1$ *k*-points [45]. Atomic positions were fully relaxed in all cases, using the conjugated gradient (CG) minimization technique.

In a preliminary analysis, we studied the unsupported H_2, PdH, Pd_2, and Pd_2H_2 systems in order to verify the accuracy of the method. Following previous theoretical works about isolated Pd_2H_2 systems [46,47], we evaluated the three most stable approach modes between the H_2 molecule and the Pd_2 dimer (see Fig. 1). The planar rhomboid complex I (Fig. 1a) has the H–H bond dissociated and comes from a perpendicular approach mode for the H_2 molecule toward the center of the Pd–Pd bond. The planar trapezoidal structure II (Fig. 1b) corresponds to a parallel interaction between H_2 and Pd_2, which elongates the H–H bond but does not dissociate it. Finally, the perpendicular H_2 approach along the axis of the dimer gives the complex IIIA (Fig. 1c) that is similar to the one formed by a single Pd atom with a relaxed H–H bond. We have also considered an additional structure called IIIB (see Fig. 1d) to make further comparison with the adsorbed case.

The graphene sheet is modeled using a $7.39 \times 8.53 \times 20$ $Å^3$ tetragonal unit cell consisting of 24 C atoms in a plane honeycomb structure [37]. A big modulus cell parameter in the normal direction to the carbon layer was chosen in order to avoid the interaction among images in adjacent cells. After the optimization process, we obtained a lattice constant of 2.459 Å, in full agreement with the experimental value [48].

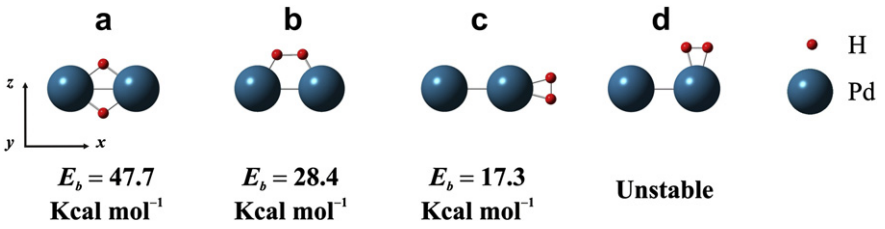

Fig. 1 – Free Pd_2H_2 complexes studied. (a) Structure I. (b) Structure II. (c) Structure IIIA. (d) Structure IIIB (frozen geometry as adsorbed on graphene). Binding energies were calculated according to $E_b = E(H_2) + E(Pd_2) - E(Pd_2H_2)$.

We examined the adsorption of the Pd_2 dimer on graphene using two Pd atoms per unit cell parallel to the carbon surface in three different adsorption sites: bridge (Fig. 2a), C–C bonds midpoint; hollow (Fig. 2b), carbon hexagons center; and top (Fig. 2c), directly above C atoms. As suggested in the literature [49,50], we also located the Pd_2 dimer perpendicular to the surface on the above mentioned adsorption sites. After determining the most stable Pd_2/graphene geometries, we investigated hydrogen adsorption, considering the three above mentioned Pd_2H_2 coordination structures analyzed in the unsupported case. These complexes were placed on preferential adsorption sites on graphene (see Figs. 3 and 4 for the bridge and top sites, respectively), with all Pd and H atoms located on a same plane, parallel (Figs. 3a, c, e and 4a, c, e) and perpendicular (Figs. 3b, d, f and 4b, d, f) to the carbon layer.

After relaxation, we computed the following geometrical parameters for each carbon-supported system: distance between Pd atoms (d_{Pd-Pd}); perpendicular distance between the average z coordinate of Pd and that of C atoms (z_{C-Pd}); average distance from each Pd atom to its nearest C atoms (d_{C-Pd}); average distance between adjacent Pd and H atoms (d_{Pd-H}); and distance between H atoms (d_{H-H}). We also determined the graphene surface (Δz) deformation defined as the maximum deviation in the z direction of distorted C atoms from the average position of the graphene surface.

The binding energies per Pd atom and H_2 molecule were calculated as

$$E_b(Pd) = [E(C_{24}) + 2E(Pd) - E(Pd_2/C_{24})]/2 \quad (1)$$

$$E_b(H_2) = E(Pd_2/C_{24}) + E(H_2) - E(H_2/Pd_2/C_{24}) \quad (2)$$

where $E(C_{24})$ is the total energy of the bare graphene sheet, $E(Pd)$ is the total energy of the free Pd atom, $E(H_2)$ is the total energy of the free-H_2 molecule, $E(Pd_2/C_{24})$ is the total energy of the Pd_2 dimer adsorbed on the graphene surface, and $E(H_2/Pd_2/C_{24})$ is the total energy of the H_2 molecule adsorbed on the graphene layer decorated with the Pd_2 dimer. According to these definitions, a positive binding energy corresponds to an attractive interaction.

We also followed the chemical bond evolution during the adsorption process through a conceptual tool such as overlap population (OP) that can be considered as a bonding measure between two selected atoms [51]. For that, we evaluated the OP values corresponding to H–H, H–Pd, C–C, and C–Pd bonds with a relevant participation in the adsorption, using all the previously optimized adsorption geometries. We also performed the average Mulliken orbital population analysis for H, C, and Pd atoms, in order to study the orbital contribution to the bonding.

Complementary tests were performed within the semi-empirical Atom Superposition and Electron Delocalization Tight-Binding (ASED-TB) method and the YAeHMOP package [52]. Details about this application can be found in the literature [53–56].

3. Results and discussions

3.1. *Unsupported H_2, Pd_2, and Pd_2H_2 systems*

We started computing bond lengths and binding energies (E_b) of unsupported H_2, PdH, Pd_2, and Pd_2H_2 systems because they

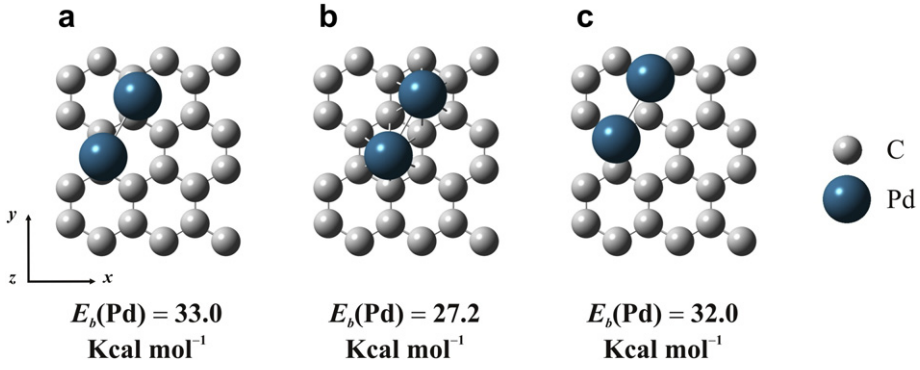

Fig. 2 – Final parallel adsorption geometries for the graphene-supported Pd_2 dimers. (a) Adsorbed on bridge sites. (b) Adsorbed on hollow sites. (c) Adsorbed on top sites. E_b(Pd) were calculated according to Eq. (1).

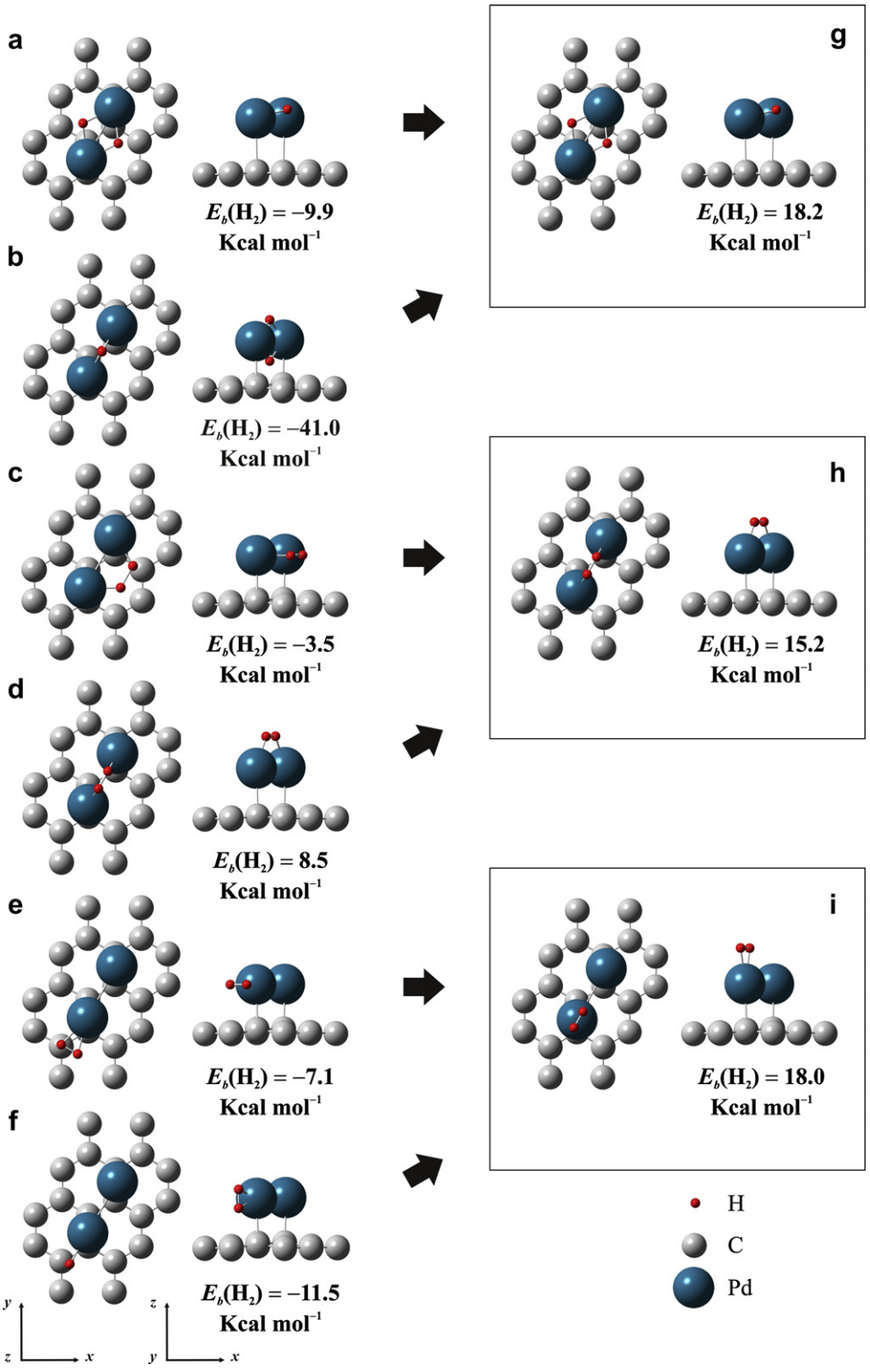

Fig. 3 – Initial adsorption geometries for the graphene-supported Pd_2H_2 complexes located on bridge sites. (a) Parallel adsorption of complex I. (b) Perpendicular adsorption of complex I. (c) Parallel adsorption of complex II. (d) Perpendicular adsorption of complex II. (e) Parallel adsorption of complex IIIA. (f) Perpendicular adsorption of complex IIIA. Final adsorption geometries (g–i) are also indicated. $E_b(H_2)$ were calculated according to Eq. (2).

can be easily compared to available experimental and theoretical data. Our optimization results are listed in Table 1, including OP and Mulliken analysis. It can be seen that reasonable estimations of experimental interatomic distances for H_2 [57], Pd_2 [58], and PdH [59] molecules were obtained, while the corresponding dissociation energies fall within the margin of experimental error [57,60,61]. Our calculations are also in full agreement with recent DFT studies [46,47].

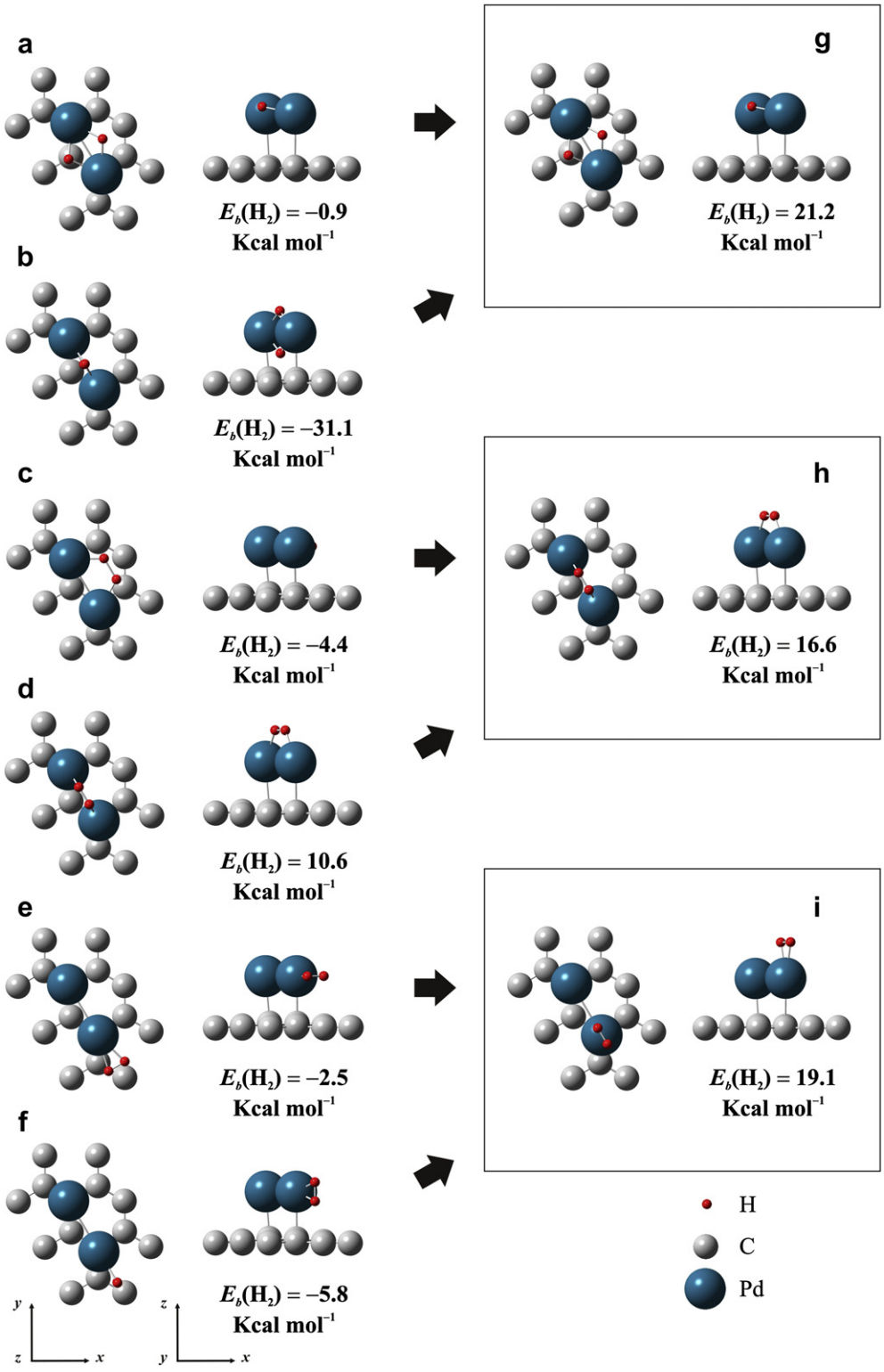

Fig. 4 – Initial adsorption geometries for the graphene-supported Pd_2H_2 complexes located on top sites. (a) Parallel adsorption of complex I. (b) Perpendicular adsorption of complex I. (c) Parallel adsorption of complex II. (d) Perpendicular adsorption of complex II. (e) Parallel adsorption of complex IIIA. (f) Perpendicular adsorption of complex IIIA. Final adsorption geometries (g–i) are also indicated. $E_b(H_2)$ were calculated according to Eq. (2).

We can see from E_b values in Table 1 that the most stable free Pd_2H_2 complex is the planar rhomboid system I (Fig. 1a), with the H–H bond strongly dissociated. In the same way, Efremenko et al. [46] and Ni et al. [47] found that structure I is the most favorable Pd_2H_2 system with similar geometrical parameters, while Cui et al. [62] also reported a nonplanar configuration with an H–Pd–Pd–H dihedral angle of 168.5° and about identical interatomic distances. The planar

Table 1 – Optimal geometrical parameters, overlap population (OP) values, orbital electron occupations, and binding energies, E_b, for free-H_2, Pd_2, PdH, and Pd_2H_2 systems.

System	Bond	OP	Distance (Å)				Atom	Orbital electron occupation			E_b (kcal mol^{-1})			
			This work	DFT[a]	DFT[b]	Experimental		*s*	*p*	*d*	This work	DFT[a]	DFT[b]	Experimental
H_2	H–H	0.856	0.750	0.762	0.747	0.746[c]	H	1.000	–	–	107.0[d]	107.4	107.9	104.2[c]
Pd_2	Pd–Pd	0.157	2.548	2.526	2.615	–[e]	Pd	0.090	0.027	9.883	15.9[f]	19.1	16.6	17 ± 6[g]
PdH	Pd–H	0.668	1.543	1.540	1.555	1.54[h]	Pd	0.505	0.081	9.078	60.6[i]	54.3	51.9	55 ± 6[j]
							H	1.337	–	–				
Pd_2H_2 I[k]	Pd–Pd	0.062	2.716	2.726	2.742	–	Pd	0.328	0.072	9.505	47.7[l]	47.7	48.0	–
	Pd–H	0.309	1.693	1.674	1.681		H	1.095						
Pd_2H_2 II[k]	Pd–Pd	0.106	2.649	2.647	2.682	–	Pd	0.252	0.004	9.789	28.4[l]	29.7	26.5	–
	Pd–H	0.226	1.612	1.602	–		H	0.955	–	–				
	H–H	0.520	1.060	1.033	1.038									
Pd_2H_2 IIIA[k]	Pd–Pd	0.081	2.705	2.775	2.590	–	Pd farthest to H_2	0.033	0.010	9.929	17.3[l]	16.3	14.3	–
	Pd–H	0.104	1.742	1.700	1.845		Pd closest to H_2	0.224	0.010	9.888				
	H–H	0.707	0.875	0.872	0.810		H	0.953	–	–				
Pd_2H_2 IIIB[k]	Pd–Pd	0.081	2.705	–	–	–	Pd farthest to H_2	0.116	0.010	9.966	unstable	–	–	–
	Pd–H	0.111	1.742				Pd closest to H_2	0.234	0.010	9.774				
	H–H	0.696	0.875				H	0.946	–	–				

a Ref. [46].
b Ref. [47].
c Ref. [57].
d $E_b = 2E(H) - E(H_2)$.
e Not experimental data available; the measured Pd–Pd bond in $[Pd_2(PMe_3)_6][hfac]_2$ is 2.598 Å [58].
f $E_b = 2E(Pd) - E(Pd_2)$.
g Ref. [60].
h Ref. [59].
i $E_b = E(H) + E(Pd) - E(PdH)$.
j Ref. [61].
k Pd_2H_2 systems I–III are presented in Fig. 1.
l $E_b = E(H_2) + E(Pd_2) - E(Pd_2H_2)$.

trapezoidal structure II (Fig. 1b), with the H–H bond parallel to the dimer and elongated to 1.060 Å, is 40.5% more unstable than the dissociative adsorption of H_2 on Pd_2 and is the second in order of stability. Finally, coordination structure IIIA (Fig. 1c) from the perpendicular H_2 approach along the axis of the Pd_2 dimer has a less modified H–H bond and a binding energy that is 63.5% lower than in complex I. Ni et al. [47] reported similar molecularly adsorbed H_2 structures II and IIIA and expected, through the analysis of the corresponding vibrational modes, that both complexes could transform to dissociative state I. Thus, earlier DFT studies suggest that the Pd_2 dimer is able to break the H–H bond and to form a very stable dissociative structure, in contrast to H_2 interaction with a single Pd atom where the most stable coordination structure is a molecular complex.

In agreement with these theoretical findings, infrared spectra recorded during matrix isolation experiments performed by Andrews et al. [63], complemented with DFT geometry and frequency calculations, have shown that thermally evaporated and laser-ablated individual Pd atoms interact with H_2 in excess argon to form a side-bonded $Pd(H_2)$ complex that reacts spontaneously with a second Pd atom to originate two Pd_2H_2 coordination structures: on the one hand, a very stable $(PdH)_2$ rhomboid ring with no H–H bond and structural parameters similar to those of our complex I and, on the other hand, a planar $Pd–Pd(H_2)$ transition state stabilized by the argon matrix and completely converted to another species by visible photoexcitation that can be assigned to our complex III. Therefore, Andrews' experiments clearly prove that one neutral Pd atom in the cold matrix cannot be inserted into a H_2 molecule but two Pd atoms dissociate H_2 to form a rhomboid $(PdH)_2$ system without activation energy.

Table 1 also summarizes our bonding analysis for all the unsupported systems studied. The results show that the Pd–Pd bond is significantly weakened during the interaction between Pd_2 and H_2 according to the different approach modes. When the Pd_2H_2 coordination structure I is formed, the H–H bond is dissociated and strong Pd–H interactions are revealed; as a result the Pd–Pd OP is decreased by 60.8% with respect to the free Pd_2 dimer. The parallel approach, which originates the trapezoidal complex II with moderate Pd–H interactions, decreases the bond OP values by 39.3% and 32.6% that correspond, respectively, to the isolated H_2 and Pd_2 reactants. Mulliken analysis by Efremenko et al. [46] also indicated that H atoms still remain to be significantly bonded in this structure. Finally, during the formation of the asymmetric $Pd_2(H_2)$ system III, we detected limited Pd–H interactions and a weakening of only 17.3% in the H–H bond with a Pd atom mainly involved in the H_2 bonding. The Pd–Pd OP becomes 48.4% smaller than that of the free Pd_2 dimer.

Mulliken analysis in Table 1 indicates that Pd_2H_2 complex I orbital populations are very similar to those of the PdH system, with a significant *p* contribution to the bonding, showing the correspondence in Pd–H interaction. These orbital occupations are in agreement with DFT calculations made by Cui et al. [62] who also suggested that, upon the perpendicular approach, Pd_2 is able to activate the H–H bond without a barrier because its lowest unoccupied molecular orbital (LUMO) has a correct symmetry to accept electron density from H_2 σ orbital. These authors also found that this mechanism differs, for example, from the case of the Pt_2 dimer, where the H_2 activation takes place at first preferentially on a single Pt atom [62]. Moreover, the reduction in Pd 4*d* electronic density and the increase in Pd 5*s* and 5*p* occupation are much less significant for the $Pd_2(H_2)$ coordination structures II and III, where the H–H bond is not broken (see Table 1). It should also be noted that the orbital populations for the Pd atom non-interacting with the H_2 molecule in complex III present almost no changes.

3.2. *Graphene-supported Pd_2 system*

Our results for Pd_2 dimer parallel approach geometrical and bonding characterization toward the graphene plane are shown in Table 2. The highest binding energies per Pd atom, E_b(Pd), belong to parallel Pd_2/graphene systems with both Pd atoms adsorbed on bridge (Fig. 2a) or top (Fig. 2c) sites, while a less stable Pd-graphene interaction is developed when the two Pd atoms are located on hollow sites (Fig. 2b). Similar adsorption geometry and energy (d_{Pd-Pd} = 2.75 Å, d_{C-Pd} = 2.26 Å, z_{C-Pd} = 2.15 Å, E_b(Pd) = 29.5 kcal mol^{-1}) were found on the bridge site of graphene by Cabria et al. [49], using a GGA-DFT method. In previous works, we reported the same trend E_b(bridge) ~ E_b(top) >E_b(hollow) for the adsorption of individual Pd atoms on graphene, by means of both DFT [37] as ASED-TB [53] calculations.

We also examined the perpendicular interaction between the Pd_2 dimer and the carbon surface. Adsorption energies for Pd_2 perpendicular adsorption on bridge, top and hollow sites have been found to be 24.2, 23.5 and 21.2 kcal mol^{-1}, respectively. In this way, the perpendicular approach mode involves lower E_b(Pd) for all sites considered on graphene and parallel adsorption becomes the preferential interaction mode between Pd_2 and graphene. Cabria et al. [49] and, more recently, Thapa et al. [50] have found an analogous behavior. According to these results, we only examined bonding changes for the parallel Pd_2/graphene configuration.

Table 2 shows that new C–Pd bonds are formed after parallel Pd_2 adsorption on graphene. The strongest C–Pd interactions correspond to adsorption on top sites, while those on bridge positions are weaker. It should be noted that the adsorption of the Pd_2 dimer on top sites implicates only two C atoms directly bonded to strong interactions. We found that in this case the C–Pd OP values on nearby C atoms are very small, while the adsorption on bridge sites involves four C atoms (two for each Pd atom) with important OP values. Consequently, Pd_2 adsorption results as favorable on bridge as on top sites, in agreement with the previous comparison for the corresponding E_b(Pd).

At the same time, Pd–Pd interaction is strongly weakened during parallel Pd_2 adsorption on graphene. Thus, the Pd–Pd bond elongates from 2.55 Å in vacuum to approximately 2.76 Å after the adsorption process. The corresponding OP value decreases up to 27.9% when the dimer is located on bridge and top sites and about 40.6% when the adsorption takes place on hollow sites (compare Table 1 vs. Table 2). The graphene surface is also affected after Pd_2 decoration and changes are subtle. In effect, OP values belonging to C–C bonds near decoration points decreased 4.9%, 4.1%, and 1.5% on bridge, top and hollow sites, respectively, showing once again that the strongest C–Pd interactions are developed on bridge and

Table 2 – Optimal geometrical parameters, overlap population (OP) values, orbital electron occupations, and binding energies per Pd, E_b(Pd), for graphene-supported Pd_2 dimers and two single Pd atoms.

System	Sites	Bond	OP	Distance (Å)	Atom	Orbital electron occupation			E_b(Pd)[a] (Kcal mol^{-1})
						s	*p*	*d*	
Pd_2/graphene (parallel orientation)[b]	Bridge	Pd–Pd	0.116	2.756	Pd	0.310	0.039	9.826	33.0
		C–Pd	0.118	2.246	C	1.188	2.735	–	
		C–C	0.957	1.442					
	Hollow	Pd–Pd	0.093	2.766	Pd	0.206	0.061	9.877	27.2
		C–Pd	0.024	2.583	C	1.176	2.787	–	
		C–C	0.994	1.429					
	Top	Pd–Pd	0.113	2.757	Pd	0.302	0.040	9.848	32.0
		C–Pd	0.159	2.176	C	1.187	2.730	–	
		C–C	0.968	1.438					
2Pd/graphene	Bridge	Pd–Pd	0.000	4.865	Pd	0.269	0.015	9.881	27.0
		C–Pd	0.116	2.237	C	1.186	2.745	–	
		C–C	0.958	1.440					
	Hollow	Pd–Pd	0.000	4.991	Pd	0.184	0.056	9.906	21.7
		C–Pd	0.026	2.505	C	1.176	2.787	–	
		C–C	0.994	1.430					
	Top	Pd–Pd	0.000	4.924	Pd	0.267	0.011	9.891	26.1
		C–Pd	0.151	2.138	C	1.188	2.731	–	
		C–C	0.972	1.434					

a E_b(Pd) was calculated according to Eq. (1). For the 2Pd/graphene systems, $E(Pd_2/C_{24})$ was replaced by $E(2Pd/C_{24})$.
b Final parallel Pd_2/graphene systems are shown in Fig. 2.

top sites. In all cases, the elongation of C–C bonds during parallel Pd_2 adsorption is lower than 1.4%, and no significant deformation of the graphene surface was found ($\Delta z < 0.2$ Å).

Mulliken orbital populations listed in Table 2 reveal that a donor-acceptor interaction between Pd_2 and graphene is present during the parallel approach mode: Pd 5*s* orbital accepts a large electron density from the nearest C atoms and Pd 4*d* orbitals donate some electron density in the opposite direction. Simultaneously, with regard to average C $2s^{1.167}2p^{2.827}$ population in the bare surface, the electron density for C 2*p* orbitals decreases significantly after the adsorption process, while C 2*s* orbitals populate to a lesser extent. These results indicate that the main C–Pd overlap comes from the interaction between C 2*p* and Pd 5*s* orbitals, with an important role of C $2p_z$ orbitals that are perpendicular to the surface. A similar interpretation has been presented in the case of adsorption of individual Pd atoms on graphene [37]. It can be seen from Table 2 that adsorptions on bridge or top sites, where the strongest C–Pd interactions are developed, involve higher donation from Pd 4*d* to C 2*s* orbitals and, especially, a back-donation from C 2*p* to Pd 5*s* orbitals that is more intense than those occurring during adsorption on hollow locations. Efremenko and Sheintuch [64] have mentioned a similar bonding scheme for Pd_2 and other small palladium clusters supported on several coordination positions of activated carbon through semi-empirical and DFT calculations.

Table 2 also lists adsorption results for two individual Pd atoms located on remote sites on the graphene surface. In this case, without a Pd–Pd interaction, there is also an increase in Pd 5*s* electronic density and a reduction in Pd 4*d* orbital occupation. These changes are almost as strong as those of the parallel graphene-supported dimer (compare, for example, Mulliken populations for 2Pd/graphene and parallel Pd_2/graphene systems on bridge sites). As a consequence, donation from Pd 4*d* orbitals to the support and back-donation to Pd 5*s* orbitals has almost the same extent for this dimer approach as for the separated adsorption of two Pd atoms. Equally, the E_b(Pd) of the parallel adsorption of Pd_2 is only up to 6 kcal mol^{-1} bigger than that of single Pd atoms on graphene. These results indicate that the adsorption is rather stronger when two Pd atoms occupy second neighbor positions so the dimerization effect is weak. On the other hand, a previous theoretical study suggests that early TMs such as Ti show a strong preference to cluster when they are adsorbed on carbon surfaces [34]. In this way, considering the high surface area of graphene and other carbon supports, we could infer that, at low loadings, a large part of Pd decoration exists in an atomically dispersed state. A similar conclusion was presented first by Efremenko and Sheintuch [64] and then by Xiao et al. [31], comparing binding energies of Pd atoms and dimers adsorbed on activated carbon or CNTs. Recent combined experimental and theoretical studies provided unambiguous identification of isolated Pd atoms occurring in the carbon matrix that coexist with larger Pd particles [65,66].

3.3. *Graphene-supported Pd_2H_2 system*

Finally, we studied the adsorption on graphene of the previously studied Pd_2H_2 complexes. Taking into account the results found in Section 3.2, we only considered the parallel adsorption approach of the Pd_2 dimer on bridge and top sites that show higher E_b(Pd) and stronger C–Pd interactions than adsorption onto hollow locations. Pd and H atoms from different Pd_2H_2 systems were placed on a parallel or perpendicular plane with regard to the graphene surface and, then, all atomic positions were fully relaxed. Table 3 shows structural, energetic and bonding results.

Table 3 – Optimal geometrical parameters, overlap population (OP) values, orbital electron occupations, and binding energies per H_2, $E_b(H_2)$, for graphene-supported Pd_2H_2 systems.

System[a]	Sites	Bond	OP	Distance (Å)	Atom	Orbital electron occupation			$E_b(H_2)$ (Kcal mol^{-1})[b]
						s	*p*	*d*	
Pd_2H_2/graphene I	Bridge	Pd–Pd	0.048	2.747	Pd	0.337	0.103	9.548	18.2
		C–Pd	0.037	2.706	C	1.172	2.803	–	
		C–C	1.000	1.426	H	1.083	–	–	
		Pd–H	0.290	1.721					
	Top	Pd–Pd	0.043	2.741	Pd	0.339	0.112	9.567	21.2
		C–Pd	0.080	2.472	C	1.175	2.792	–	
		C–C	0.992	1.429	H	1.072	–	–	
		Pd–H	0.280	1.730					
Pd_2H_2/graphene II	Bridge	Pd–Pd	0.072	2.729	Pd	0.282	0.044	9.825	15.2
		C–Pd	0.090	2.363	C	1.182	2.766	–	
		C–C	0.978	1.436	H	0.962	–	–	
		Pd–H	0.116	1.730					
		H–H	0.674	0.925					
	Top	Pd–Pd	0.069	2.744	Pd	0.278	0.041	9.836	16.6
		C–Pd	0.115	2.302	C	1.180	2.768	–	
		C–C	0.985	1.431	H	0.960	–	–	
		Pd–H	0.123	1.719					
		H–H	0.664	0.933					
Pd_2H_2/graphene III	Bridge	Pd–Pd	0.103	2.760	Pd farthest to H_2	0.303	0.043	9.854	18.0
		C–Pd	0.106	2.276	Pd closest to H_2	0.351	0.046	9.751	
		C–C	0.969	1.439	C	1.186	2.754	–	
		Pd–H	0.096	1.732	H	0.962	–	–	
		H–H	0.719	0.864					
	Top	Pd–Pd	0.099	2.760	Pd farthest to H_2	0.283	0.041	9.877	19.1
		C–Pd	0.127	2.242	Pd closest to H_2	0.339	0.040	9.771	
		C–C	0.983	1.428	C	1.180	2.755	–	
		Pd–H	0.100	1.724	H	0.960	–	–	
		H–H	0.714	0.866					

a Final Pd_2H_2/graphene I, II and III geometries are shown in Fig. 3 (bridge sites) and 4 (top sites).
b $E_b(H_2)$ was calculated according to Eq. (2).

A similar binding energy per H_2 molecule, $E_b(H_2)$, was found for Pd_2H_2 coordination structure I adsorption on bridge and top sites, for both initial approach modes (see Figs. 3g and 4g). In all cases, the dissociative Pd_2H_2 complex is finally adsorbed in parallel to the graphene layer. This behavior suggests the existence of a destabilized effect when H atoms are located between the Pd_2 dimer and the support, therefore, the strongest Pd–H interaction seems to develop out of the carbon surface. In this way, the Pd–H distance and OP value of the supported Pd_2H_2 complex I are only slightly longer and lower, respectively, than those of the free coordination structure (see Tables 1 and 3). As a result of C–Pd interaction, the Pd–Pd bond is elongated during the parallel Pd_2H_2 adsorption process and the corresponding OP decreased 22.3%. However, the C–Pd overlap is strongly weakened in this case with regard to the Pd_2/graphene system, because Pd atoms are mainly involved in Pd–H bonding (compare Tables 2 and 3).

Mulliken populations for the adsorbed Pd_2H_2 complex I, listed in Table 3, also show that H atoms modified the C–Pd bonding, thus reducing both donation from Pd 4*d* to C 2*s* orbitals and back-donation from C 2*p* to Pd 5*s* orbitals. In effect, electron occupations of C 2*s* and 2*p* orbitals are respectively decreased and increased when H atoms are present. According to this, small C–Pd OP values are obtained. At the same time, due to carbon support, H 1*s* orbitals are less populated than in the isolated complex, and H–Pd interactions are weaker.

Regarding the molecular hydrogen $Pd_2(H_2)$ systems adsorbed on graphene, we can see from Table 3 that $E_b(H_2)$ for complex III is rather higher than that for configuration II, in contrast to the gas-phase situation in which coordination structure II is ~40% more stable (see Table 1). Moreover, after adsorption on graphene these systems are almost as stable as complex I that is clearly the most favorable isolated alternative. Carbon support could thus provide an additional stabilization on not dissociative $Pd_2(H_2)$ complexes.

Although several initial adsorption geometries were tested, a perpendicular final adsorption arrangement was always obtained between $Pd_2(H_2)$ structures II or III and the graphene plane (see Figs. 3h, i and 4h, i). Therefore, we could assume that the previously mentioned support stabilization effect is only possible when H atoms are located away from the carbon surface. Previous DFT studies [30,31] about the adsorption of one or several H_2 molecules on a (8,0) SWCNT uniformly decorated with individual Pd atoms seem to confirm this hypothesis.

The Mulliken orbital analysis showed in Table 3 reveals that C–Pd donation and back-donation rates during $Pd_2(H_2)$ complex II adsorption almost equal the values of the free-H Pd_2/graphene system (see Table 2). As a result, C–Pd

Table 4 – Hydrogen molecular orbital electron occupations for free and graphene-supported PdH_2 and Pd_2H_2 systems.

System	Site	Orbital electron occupation	
		H_2 σ	H_2 σ^*
H_2	–	2.000	0.000
PdH_2[a]	–	1.849	0.038
Pd_2H_2 II[b]	–	1.770	0.139
Pd_2H_2 IIIB[b]	–	1.860	0.031
PdH_2/graphene[a]	Bridge	1.894	0.026
	Top	1.898	0.028
Pd_2H_2/graphene II[c]	Bridge	1.868	0.056
	Top	1.861	0.060
Pd_2H_2/graphene III[c]	Bridge	1.890	0.035
	Top	1.884	0.035

a Ref. [37].
b Unsupported Pd_2H_2 systems II and IIIB are shown in Fig. 1.
c Final Pd_2H_2/graphene II and III geometries are shown in Fig. 3 (bridge sites) and 4 (top sites).

interactions resulting after $Pd_2(H_2)$ complex II adsorption are significantly stronger than those of carbon-supported dissociative structure I. Simultaneously, Pd–Pd OP belonging to $Pd_2(H_2)$ configuration II decreased 31.7% and 35.4% on bridge and top sites, respectively, compared to the vacuum value (see Tables 1 and 3). Complex II interaction with the graphene sheet also enlarges the Pd–H distance producing a substantial decrease in the corresponding OP and, simultaneously, an increase in H 1*s* orbital population and H–H overlap, compared to the unsupported structure.

The preferential adsorption geometry of $Pd_2(H_2)$ coordination structure III on graphene, showed in Figs. 3i and 4i for the bridge and top sites, respectively, also has a stretched Pd–Pd bond with respect to the free system in an analogous geometry as showing in Fig. 1d (compare Tables 1 and 3). This elongation is due to C–Pd interactions, which are stronger than for complex II adsorption and involve more important donation to C 2*s* orbitals and higher back-donation from C 2*p* orbitals, as can be seen in the Mulliken analysis for C atoms listed in Table 3. As in complex II adsorption, C–Pd interactions developed during the perpendicular approach between $Pd_2(H_2)$ III and graphene are weaker than those of the Pd_2/graphene system, where H atoms are not present (see also Table 2). In this case, the interaction with the support does not alter H–H and Pd–H bonds significantly, the OP values of which are almost the same as in the free complex.

Finally, we evaluated hydrogen molecular orbital occupation for free and adsorbed $Pd_2(H_2)$ structures II and III summarized in Table 4, in order to get more insight into the bonding mechanism between the graphene-supported Pd_2 dimer and H_2 molecule. The results for the non-dissociative $Pd(H_2)$ system, so-called Kubas complex [24], are also included for comparison. From Tables 3 and 4, we can see that the Pd_2–H_2 interaction involves two intermolecular donor-acceptor delocalizations: the σ donation, from H_2 σ to Pd 5*s* orbitals, and the π back-donation, from Pd 4*d* to H_2 σ^* orbitals. Fig. 5 presents simplified wave function plots showing this donation/back-donation scheme. In effect, the σ bonding

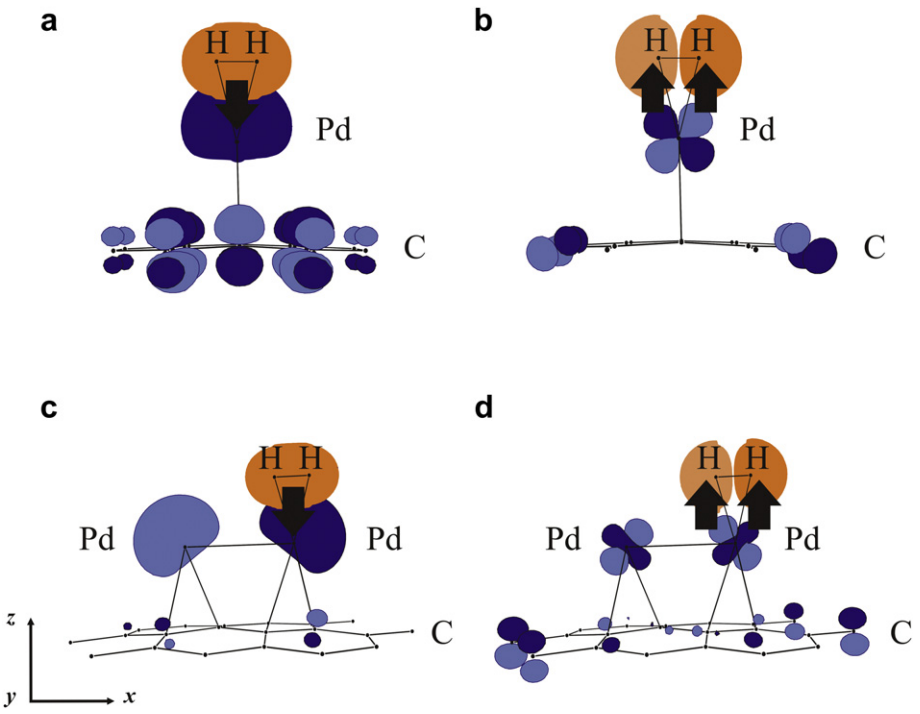

Fig. 5 – Simplified wave function plots showing the intermolecular donor-acceptor delocalizations involved during the Pd–H_2 interaction. (a) σ donation in the graphene-supported PdH_2 Kubas complex. (b) π back-donation in the graphene-supported PdH_2 Kubas complex. (c) σ donation in the graphene-supported Pd_2H_2 complex III. (d) π back-donation in the graphene-supported Pd_2H_2 complex III.

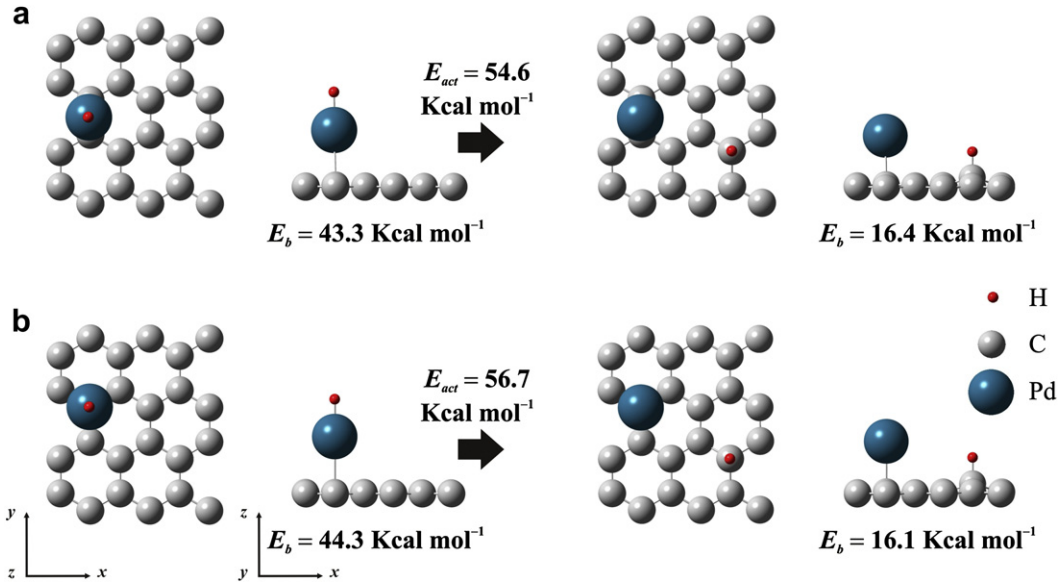

Fig. 6 – Adsorption geometries for the migration of an H atom from an adsorbed Pd atom to the graphene surface. (a) Pd atom adsorbed on a bridge site. (b) Pd atom adsorbed on a top site. Binding energies were calculated according to $E_b = E(Pd/C_{24}) + E(H) - E(H/Pd/C_{24})$. Energy barriers ($E_{act}$) are also indicated for both H migrations.

orbital of the H_2 molecule increases its electron occupation during adsorption of both $Pd_2(H_2)$ structures on the graphene layer, being this increment considerably higher for complex II. At the same time, the electron population of the H_2 molecule σ^* antibonding orbital is reduced when Pd_2H_2 complex II is adsorbed on graphene and is less increased for adsorbed configuration III. Therefore, the presence of the carbon support seems to reduce both the σ donation and π back-donation after interaction with Pd_2H_2 system II, resulting in H–H bond strengthening. Contrarily, in the case of complex III adsorption, σ donation is reduced but π back-donation increases and the H–H overlap shows only small changes. Adsorption of the $Pd_2(H_2)$ structure II on graphene is thus similar to that of the PdH_2 Kubas complex, where the H–H is also strengthened [37]. Moreover, comparing the H_2 molecular orbital occupation of graphene-supported $Pd(H_2)$ and $Pd_2(H_2)$ systems in Table 4, it should be noted that a second Pd atom adsorbed near $Pd(H_2)$ enhances both σ donation and π back-donation, thus destabilizing dihydrogen interaction. However, due to the fact that these changes are small, the Pd clustering effect could not affect the bonding mechanism of stored hydrogen in Pd-doped graphene significantly.

A recent DFT and experimental study [65] supports our findings. The calculations reveal that a single Pd atom can form Kubas-type complexes by binding up to three H_2 molecules. The excess hydrogen uptake measured experimentally makes Kubas binding as a viable mechanism (along with hydride formation and physisorption to carbon support). The authors finally conclude that the role of hydrogen spillover in Pd-carbon nanofibers may be smaller than previously thought at low and moderated pressures. Parambhath et al. [67] have recently presented experimental evidence for the spillover mechanism in palladium decorated hydrogen exfoliated functionalized graphene. In this case Pd particles were estimated to be 6.6 nm and the surface contains several types of defects and functionalized groups (–OH, $-CH_2$, –C=O, –COOH). In a related work, Psofogiannakis and Foundakis [68] simulated H-spillover using a Pt/coronene system concluding that a very large energy barrier (>50 kcal mol^{-1}) have to be overcame for H migration from Pt to the carbon surface. We have calculated the energy for the migration of an H atom from a Pd atom adsorbed on bridge or top sites to the graphene surface (see Fig. 6). Our results are close to that reported in Ref. [68]. All these evidences indicate that the spillover is a phenomena far from well understood and will be the subject of a forthcoming study. Other important thermodynamic quantities can be computed as a function of temperature and pressure using DFT codes from a demanding vibrational analysis to determine entropy and rate constants [68].

4. Conclusions

In this work, we have performed DFT calculations in order to study the adsorption of Pd_2 dimers and Pd_2H_2 complexes on a graphene layer. First, we found that a Pd_2 dimer is preferentially adsorbed in a parallel configuration on the second neighbor bridge site -at the midpoint of a C–C bond- or on top sites -above a C atom- on graphene. This interaction becomes slightly stronger than the adsorption of two single Pd atoms located on distant sites. In presence of dihydrogen, both a rhomboid $(PdH)_2$ ring without H–H bond and not dissociative $Pd_2(H_2)$ systems are originated. In all cases, Pd_2H_2 adsorption geometries with H atoms located away from the carbon surface are favored, developing similar binding energies for bridge and top sites. Moreover, we found, by means of

Mulliken analysis, that after Pd_2H_2 adsorption C–Pd interaction results weakened with regard to the free-H Pd_2/graphene system, thus reducing both donation from Pd 4*d* to C 2*s* orbitals and back-donation from C 2*p* to Pd 5*s* orbitals. At the same time, and due to the interaction with the carbon sheet, Pd–Pd and Pd–H bonds are elongated with respect to isolated coordination structures. We also found that the Pd_2–H_2 bonding mechanism in non-dissociative adsorbed complexes, which involves σ donation from H_2 σ to Pd 5*s* orbitals and π back-donation from Pd 4*d* to H_2 σ^* orbitals, leads to a strengthening of the H–H bond with regard to free $Pd_2(H_2)$ structures; however, the dihydrogen interaction is weaker than that of the supported $Pd(H_2)$ Kubas complex. Our findings indicate that Pd_2 dimers adsorbed on graphene after a parallel approach can dissociate the H_2 molecule to form a very stable $(PdH)_2$ configuration, contrary to supported individual Pd atoms, which preferably originates a molecular PdH_2 complex. However, formation of not dissociative $Pd_2(H_2)$ complexes is also possible, so the dimerization effect for carbon-supported Pd atoms could not impact negatively on the hydrogen uptake of Pd-decorated graphene-based structures.

Acknowledgments

The authors thank R. Faccio, M. I. Rojas and E. P. M. Leiva for their advice during the SIESTA program implementation. This work was supported by SGCyT-UNS, PICT 1770, PIP-CONICET 11220090100785 and PAE 22711. I. López-Corral is a CONICET research fellow. A. Juan, M. A. Volpe, E. Germán and G. P. Brizuela are CONICET researchers.

REFERENCES

[1] Ströbel R, Garche J, Moseley PT, Jörissen L, Wolf G. Hydrogen storage by carbon materials. J Power Sources 2006;159:781–801.
[2] Yürüma Y, Taralp A, Veziroglu TN. Storage of hydrogen in nanostructured carbon materials. Int J Hydrogen Energy 2009;34:3784–98.
[3] Wang L, Yang RT. New sorbents for hydrogen storage by hydrogen spillover: a review. Energy Environ Sci 2008;1:268–79.
[4] Li Y, Yang RT. Hydrogen storage on platinum nanoparticles doped on superactivated carbon. J Phys Chem C 2007;111:11086–94.
[5] Zacharia R, Rather S, Hwang SW, Nahm KS. Spillover of physisorbed hydrogen from sputter-deposited arrays of platinum nanoparticles to multi-walled carbon nanotubes. Chem Phys Lett 2007;434:286–91.
[6] Leela Mohana Reddy A, Ramaprabhu S. Hydrogen adsorption properties of single-walled carbon nanotube-nanocrystalline platinum composites. Int J Hydrogen Energy 2008;33:1028–34.
[7] Kim HS, Lee H, Han KS, Kim JH, Song MS, Park MS, et al. Hydrogen storage in Ni nanoparticle-dispersed multiwalled carbon nanotubes. J Phys Chem B 2005;109:8983–6.
[8] Lee JW, Kim HS, Lee JY, Kang JK. Hydrogen storage and desorption properties of Ni-dispersed carbon nanotubes. Appl Phys Lett 2006;88:143126.
[9] Zielinski M, Wojcieszak R, Monteverdi S, Mercy M, Bettahar MM. Hydrogen storage in nickel catalysts supported on activated carbon. Int J Hydrogen Energy 2007;32:1024–32.
[10] Lueking A, Yang RT. Hydrogen spillover from a metal oxide catalyst onto carbon nanotubes: implications for hydrogen storage. J Catal 2002;206:165–8.
[11] Lueking A, Yang RT. Hydrogen storage in carbon nanotubes: residual metal content and pretreatment temperature. AIChE J 2003;49:1556–68.
[12] Lupu D, Biris AR, Misan I, Jianu A, Holzhuter G, Burkel E. Hydrogen uptake by carbon nanofibers catalyzed by palladium. Int J Hydrogen Energy 2004;29:97–102.
[13] Yoo E, Gao L, Komatsu T, Yagai N, Arai K, Yamazaki T, et al. Atomic hydrogen storage in carbon nanotubes promoted by metal catalysts. J Phys Chem B 2004;108:18903–7.
[14] Zacharia R, Kim KY, Fazle Kibria AKM, Nahm KS. Enhancement of hydrogen storage capacity of carbon nanotubes via spill-over from vanadium and palladium nanoparticles. Chem Phys Lett 2005;412:369–75.
[15] Lachawiec AJ, Qi GS, Yang RT. Hydrogen storage in nanostructured carbons by spillover: bridge-building enhancement. Langmuir 2005;21:11418–24.
[16] Li YW, Yang RT. Significantly enhanced hydrogen storage in metal-organic frameworks via spillover. J Am Chem Soc 2006;128:726–7.
[17] Yang FH, Lachawiec AJ, Yang RT. Adsorption of spillover hydrogen atoms on single-wall carbon nanotubes. J Phys Chem B 2006;110:6236–44.
[18] Ansón A, Lafuente E, Urriolabeitia E, Navarro R, Benito AM, Maser WK, et al. Hydrogen capacity of palladium-loaded carbon materials. J Phys Chem B 2006;110:6643–8.
[19] Lipson AG, Lyakhov BF, Saunin EI, Tsivadze AY. Evidence for large hydrogen storage capacity in single-walled carbon nanotubes encapsulated by electroplating Pd onto a Pd substrate. Phys Rev B 2008;77:081405.
[20] Campesi R, Cuevas F, Gadiou R, Leroy E, Hirscher M, Vix-Guterl C, et al. Hydrogen storage properties of Pd nanoparticle/carbon template composites. Carbon 2008;46:206–14.
[21] Wu X, Gallego NC, Contescu CI, Tekinalp H, Bhat VV, Baker FS, et al. The effect of processing conditions on microstructure of Pd-containing activated carbon fibers. Carbon 2008;46:54–61.
[22] Jewell LL, Davis BH. Review of absorption and adsorption in the hydrogen-palladium system. Appl Catal A 2006;310:1–15.
[23] Bhat VV, Contescu CI, Gallego NC. The role of destabilization of palladium hydride in the hydrogen uptake of Pd-containing activated carbons. Nanotech 2009;20:204011.
[24] Kubas GJ. Metal-dihydrogen and sigma-bond coordination: the consummate extension of the Dewar-Chatt-Duncanson model for metal-olefin bonding. J Organomet Chem 2001;635:37–68.
[25] Zidan R, Rao AM. DOE hydrogen program: FY 2002 Progress Report.
[26] Yildirim T, Ciraci S. Titanium-decorated carbon nanotubes as a potential high-capacity hydrogen storage medium. Phys Rev Lett 2005;94:175501.
[27] Yildirim T, Iñiguez J, Ciraci S. Molecular and dissociative adsorption of multiple hydrogen molecules on transition metal decorated C_{60}. Phys Rev B 2005;72:153403.
[28] Zhao YF, Kim YH, Dillon AC, Heben MJ, Zhang SB. Hydrogen storage in novel organometallic buckyballs. Phys Rev Lett 2005;94:155504.
[29] Durgun E, Ciraci S, Yildirim T. Functionalization of carbon-based nanostructures with light transition-metal atoms for hydrogen storage. Phys Rev B 2008;77:85405.
[30] Dag S, Ozturk Y, Ciraci S, Yildirim T. Adsorption and dissociation of hydrogen molecules on bare and functionalized carbon nanotubes. Phys Rev B 2005;72:155404.

[31] Xiao H, Li SH, Cao JX. First-principles study of Pd-decorated carbon nanotube for hydrogen storage. Chem Phys Lett 2009; 483:111–4.
[32] Zhang Y, Dai H. Formation of metal nanowires on suspended single-walled carbon nanotubes. Appl Phys Lett 2000;77: 3015–7.
[33] Zhang Y, Franklin NW, Chen RJ, Dai H. Metal coating on suspended carbon nanotubes and its implication to metal-tube interaction. Chem Phys Lett 2000;331:35–41.
[34] Sun Q, Wang Q, Jena P, Kawazoe Y. Clustering of Ti on a C_{60} surface and its effect on hydrogen storage. J Am Chem Soc 2005;127:14582–3.
[35] Wagemans RWP, van Lenthe JH, de Jongh PE, van Dillen AJ, de Jong KP. Hydrogen storage in magnesium clusters: quantum chemical study. J Am Chem Soc 2005;127:16675–80.
[36] Zlotea C, Cuevas F, Paul-Boncour V, Leroy E, Dibandjo P, Gadiou R, et al. Size-dependent hydrogen sorption in ultrasmall Pd clusters embedded in a mesoporous carbon template. J Am Chem Soc 2010;132:7720–9.
[37] López-Corral I, Germán E, Juan A, Volpe MA, Brizuela GP. DFT study of hydrogen adsorption on palladium decorated graphene. J Phys Chem C 2011;115:4315–23.
[38] Hohenberg P, Kohn W. Inhomogeneous electron gas. Phys Rev 1964;136. B864-BB71.
[39] Kohn W. Nobel Lecture: electronic structure of matter-wave functions and density functionals. Rev Mod Phys 1999;71: 1253–66.
[40] Perdew JP, Burke K, Ernzerhof M. Generalized gradient approximation made simple. Phys Rev Lett 1996;77:3865–8.
[41] Ordejón P, Artacho E, Soler JM. Self-consistent order-N density-functional calculations for very large systems. Phys Rev B 1996;53. R10441-R104R4.
[42] Soler JM, Artacho E, Gale JD, García A, Junquera J, Ordejón P, et al. The SIESTA method for ab initio order-N materials simulation. J Phys Condes Matter 2002;14:2745–79.
[43] Junquera J, Paz O, Sánchez-Portal D, Artacho E. Numerical atomic orbitals for linear-scaling calculations. Phys Rev B 2001;64:235111.
[44] Troullier N, Martins JL. Efficient pseudopotentials for plane-wave calculations. Phys Rev B 1991;43:1993–2006.
[45] Monkhorst HJ, Pack JD. Special points for Brillouin-zone integrations. Phys Rev B 1976;13:5188–92.
[46] Efremenko I, German ED, Sheintuch M. Density functional study of the interactions between dihydrogen and Pd_n ($n = 1$–4) clusters. J Phys Chem A 2000;104:8089–96.
[47] Ni MY, Zeng Z. Density functional study of hydrogen adsorption and dissociation on small Pdn ($n = 1$–7) clusters. J Mol Struct (Theochem) 2009;910:14–9.
[48] Baskin Y, Meyer L. Lattice constants of graphite at low temperatures. Phys Rev 1955;100:544.
[49] Cabria I, Lopez MJ, Alonso JA. Theoretical study of the transition from planar to three-dimensional structures of palladium clusters supported on graphene. Phys Rev B 2010; 81:035403.
[50] Thapa R, Sen D, Mitra MK, Chattopadhyay KK. Palladium atoms and its dimers adsorbed on graphene: first-principles study. Phys B 2011;406:368–73.
[51] Hoffmann R. Solids and surfaces. A chemist's view of bonding in extended structures. New York: VCH; 1988.
[52] Landrum GA, Glassey WV. Yet another extended Hückel molecular orbital package (YAeHMOP). YAeHMOP is freely available on the world wide web at:. Ithaca: Cornell University Press http://yaehmop.sourceforge.net/; 2004.
[53] López-Corral I, Germán E, Volpe MA, Brizuela GP, Juan A. Tight-binding study of hydrogen adsorption on palladium decorated graphene and carbon nanotubes. Int J Hydrogen Energy 2010;35:2377–84.
[54] Brizuela G, Hoffmann R. $C_5H_5^-$ on a Pt(111) surface: electronic structure and bonding. J Phys Chem A 1998;102:9618–24.
[55] Germán E, López-Corral I, Juan A, Brizuela G. A bonding study of cyclopentene (c-C_5H_8) adsorption on Ni(111) surface. J Mol Catal A 2008;290:23–9.
[56] Germán E, López-Corral I, Juan A, Brizuela G. A theoretical study of cyclopentene (c-C_5H_8) dehydrogenation to cyclopentadienyl anion (c-$C_5H_5^-$) on Ni (111). J Mol Catal A 2009;314:28–34.
[57] Weast RC, Selby SM. Handbook of Chemistry and Physics. 55th ed. Cleveland: Chemical Rubber Co.; 1974.
[58] Lin W, Wilson SR, Girolami GS. Synthesis and X-ray crystal structure of the new palladium(I) dimer $[Pd_2(PMe_3)_6][hfac]_2$ and its conversion to $[PdMe(PMe_3)_3][hfac]$ via activation of phosphorus-carbon bonds. Inorg Chem 1994;33:2265–72.
[59] Knight Jr LB, Weltner Jr W. Hyperfine interaction and chemical bonding in the PdH molecule. J Mol Spectrosc 1971;40:317–27.
[60] Lin SS, Strauss B, Kant A. Dissociation energy of Pd_2. J Chem Phys 1969;51:2282–3.
[61] Tolbert MA, Beauchamp JL. Homolytic and heterolytic bond dissociation energies of the second row group 8, 9, and 10 diatomic transition-metal hydrides: correlation with electronic structure. J Phys Chem 1986;90:5015–22.
[62] Cui Q, Musaev DG, Morokuma K. Molecular orbital study of H_2 and CH_4 activation on small metal clusters. I. Pt, Pd, Pt_2, and Pd_2. J Chem Phys 1998;108:8418–28.
[63] Andrews L, Wang XF, Alikhani ME, Manceron L. Observed and calculated infrared spectra of $Pd(H_2)_{(1,2,3)}$ complexes and palladium hydrides in solid argon and neon. J Phys Chem A 2001;105:3052–63.
[64] Efremenko I, Sheintuch M. Carbon-supported palladium catalysts. Molecular orbital study. J Catal 2003;214:53–67.
[65] Contescu CI, van Benthem K, Li S, Bonifacio CS, Pennycook SJ, Jena P, et al. Single Pd atoms in activated carbon fibers and their contribution to hydrogen storage. Carbon 2011;49:4050–8.
[66] van Benthem K, Bonifacio CS, Contescu CI, Gallego NC, Pennycook SJ. STEM imaging of single Pd atoms in activated carbon fibers considered for hydrogen storage. Carbon 2011; 49:4059–63.
[67] Parambhath VB, Nagar R, Sethupathi K, Ramaprabhu S. Investigation of spillover mechanism in palladium decorated hydrogen exfoliated functionalized graphene. J Phys Chem C 2011;115:15679–85.
[68] Psofogiannakis GM, Froudakis GE. DFT study of the hydrogen spillover mechanism on Pt-doped graphite. J Phys Chem C 2009;113:14908–15.